Small Signal Analysis of Power Systems With Wind and Energy Storage Units

Arash Jamehbozorg and Ghadir Radman

***Abstract*—A study of small signal behavior of power systems including wind generation units and energy capacitor systems (ECSs) is presented in this paper. Modeling of wind units with squirrel-cage induction generators connected to power system through a full-scale AC/AC converter and ECS unit are explained thoroughly. The ECS unit (considered in this paper) consists of electric double-layer capacitors (EDLC) and DC/AC converter. Small signal behavior of three test systems are studied and compared with one another using digital computer simulations. The three systems are: S1) WSCC 9-bus system with three conventional synchronous generators (SGs), S2) the WSCC system with one of the conventional SGs replaced by a wind energy system, and S3) the same as S2) but with the addition of an ECS unit. The study includes comparing of dominant eigenvalues, the participant state variables, and the related participation factors for the three systems. In addition, the effects of loading on the unstable modes of the system with conventional SG, wind and ECS units (system S3) are studied using the trajectory of these modes as loads are increased.**

***Index Terms*—Dynamic model, dynamic studies, energy capacitor system, wind units.**

NOMENCLATURE

Subscript q	q-axis component of the variable.
Subscript d	d -axis component of the variable.
Subscript s	Generator-side converter variables.
Subscript L	Wind unit grid-side converter variables.
Subscript e	ECS grid-side converter variables.
ω_r	Electrical angular speed of the rotor [rad/s].
J	Moment of inertia.
P	Number of poles.
T_m	Mechanical torque $[N \cdot m]$.
T_e	Electrical torque $[N \cdot m]$.
m	Modulation index of converter.
$V_{\rm dc}$	DC-link voltage [V].
ω_e	Generator electrical angular speed [rad/s].
L_m	Mutual inductance [H].
L_r	Rotor inductance [H].
λ_r	Rotor flux linkage [Wb].
R_r	Rotor resistance [Ω].
C	DC-link capacitance [F].
R_g	Wind unit filter resistance [Ω].
L_g	Wind unit filter inductance [H].
ω_g	Electrical angular speed of the grid [rad/s].
V_g	Grid voltage [V].
L_s	Stator inductance [H].
R_s	Stator resistance [Ω].
$P_{\rm in}$	Input power of the DC/AC converter [W].
$P_{\rm loss}$	Copper losses due to the filter resistance [W].
$P_{\rm ref}$	Reference value of the active power [W].
$Q_{\rm ref}$	Reference value of the reactive power [VAr].
R_f	ECS unit filter resistance [Ω].
L_f	ECS unit filter inductance [H].
$\|V_i\|$	Voltage magnitude of Bus i.
θ_i	Voltage angle of Bus i.
I_m	Synchronous generator output current.
ρ	Air density $= 1.225$ [kg/m^3].
A	Wind turbine blade surface [m^2].
C_p	Power coefficient of wind turbine.
V_w	Wind speed [m/s].
$\lambda_{\rm opt}$	Optimal tip speed ratio.
R_t	Radius of turbine blades [m].
N_g	Gear box ratio.
λ	Tip speed ratio.
β	Blade pitch angle [rad].
P_i	Active power of the load at Bus i [W].
Q_i	Reactive power of the load at Bus i [VAr].

Manuscript received October 01, 2013; revised February 06, 2014; accepted March 29, 2014. Paper no. TPWRS-01254-2013.

A. Jamehbozorg is with the Department of Electrical and Computer Engineering, California State University, Los Angeles, CA 90032 USA (e-mail: arash.jamehbozorg@calstatela.edu).

G. Radman is with the Department of Electrical and Computer Engineering, Tennessee Tech University, Cookeville, TN 38505 USA (e-mail: gradman@tntech.edu).

Color versions of one or more of the figures in this paper are available online at http://ieeexplore.ieee.org.

Digital Object Identifier 10.1109/TPWRS.2014.2321711

I. INTRODUCTION

WIND energy is one of the cheapest and cleanest sources of electrical energy. Installed capacity of wind power plants has increased from 59.3 GW in 2005 to 198 GW in 2010 with nearly $50 billion invested on wind energy in last 20 years [1]. Increased penetration of wind energy in power network is accompanied with deteriorated system dynamics (due to intermittent nature of wind speed), which should be taken into

considerations. To compensate for these deteriorations new methods and equipment should be employed.

It has been shown that energy storage systems can effectively improve power systems dynamics [2]–[10]. In recent years, storage system capacity has been increased from tens of megawatt-hours to hundreds of megawatt-hours. In California a storage facility is going to be built that can deliver a full gigawatt to the grid for 4 to 6 hours [11]. The ability of these sources to deliver/absorb large amount of power makes them a suitable choice for improving the dynamics of wind units and the overall power system. Several studies have been reported in literature related to output power smoothing of wind units connected to infinite bus using energy storage systems to compensate for wind speed fluctuations [12]–[15]. However, effects of power fluctuations of wind units on multi-machine power systems have not been investigated thoroughly.

This paper presents a study of small signal behavior of power systems including wind energy and energy capacitor systems (ECSs), which consists of electric double-layer capacitors (EDLC). The EDLC needs a simple charging mechanism and requires no protective circuits. Overcharging or over-discharging does not have negative effects on its lifespan, as it does on that of chemical batteries [16]. For computer simulation three test systems are used. For test system 1, we use the WSCC 9-bus 3-machine system [17]. For Test system 2, the synchronous generator at Bus 2 is replaced with a wind unit. For test system 3, we add an ECS unit to the test system 2. For each test system eigenvalues, participant variables, and participation factors are found and compared. Moreover, for the system containing wind and ECS units (test system 3), a thorough small signal analysis is performed.

In next section, modeling of wind and ECS units are explained. Then state-space equation of the system is formed in Section III. In Section IV, small signal characteristics of wind and ECS units are calculated and in Section V, small signal behaviors of three systems are compared.

II. System Modeling

For performing small signal analysis different components of power system should be modeled first. For synchronous generators, one-axis model presented in [17] is used. This model assumes one-mass steam turbine including four dynamic equations together with two algebraic equations. Each generator is assumed to be equipped with an IEEE DC-1A type exciter [18]. This exciter adds three more dynamic equations to the system.

Two other components, wind and ECS units, are shown in Fig. 1.

a) Modeling of Wind Unit: For wind unit, a squirrel-cage induction generator (SCIG) connected to the grid through a full-scale AC/AC converter (a combination of generator side AC/DC and grid side DC/AC converters) is used. Wind speed is modeled according to [19]. Dynamic equations of SCIG and the related converters are as follows [20]:

$$s\omega_r = \frac{P}{2J}(T_m + T_e) \tag{1}$$

$$sI_{qs} = \frac{1}{L_\sigma}\left(\frac{1}{2}m_{qs}V_{\rm dc} - RI_{qs} - \omega_e L_\sigma I_{\rm ds} - \frac{\omega_r L_m}{L_r}\lambda_r\right) \tag{2}$$

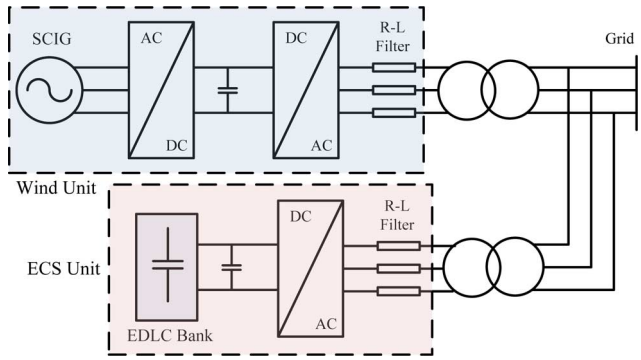

Fig. 1. Topology of wind and ECS units.

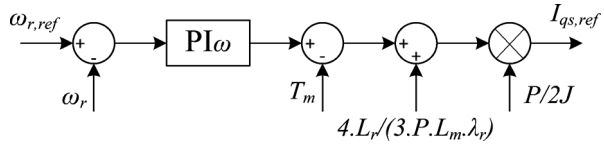

Fig. 2. Block diagram of rotor speed control loop.

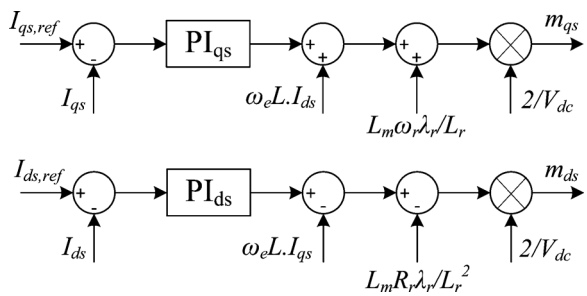

Fig. 3. Block diagram of the generator-side control loops.

$$sI_{\rm ds} = \frac{1}{L_\sigma}\left(\frac{1}{2}m_{\rm ds}V_{\rm dc} - RI_{\rm ds} + \omega_e L_\sigma I_{qs} + \frac{R_r L_m}{L_r^2}\lambda_r\right) \tag{3}$$

$$sV_{\rm dc} = \frac{3}{4C}(m_{qs}I_{qs} + m_{\rm ds}I_{\rm ds} + m_{qL}I_{qL} + m_{dL}I_{dL}) \tag{4}$$

$$sI_{qL} = \frac{1}{L_f}\left(\frac{1}{2}m_{qL}V_{\rm dc} - |V_g| - R_g I_{qL} - \omega_g L_g I_{dL}\right) \tag{5}$$

$$sI_{dL} = \frac{1}{L_f}\left(\frac{1}{2}m_{dL}V_{\rm dc} - R_g I_{dL} + \omega_g L_g I_{qL}\right) \tag{6}$$

where $L_\sigma = L_s - (L_m^2)/(L_r)$, and $R = R_s + (L_m^2)/(L_r^2)R_r$.

For generator-side converter, the control objectives are related to maximum power point tracking (MPPT) and indirect filed-orientation control [21]. Based on these strategies block diagrams of rotor speed control loop (to achieve maximum power point) and generator-side current control loops are designed as Figs. 2 and 3, respectively.

For grid-side converter, the control objectives are to maintain constant DC-link voltage and regulate the output reactive power of the wind unit. Fig. 4 shows block diagram of the DC-link voltage controller, and Fig. 5 shows block diagrams of the grid-side converter control loops. Equation (*) in Fig. 4 is defined as follows:

$$I_{qL,\rm ref} = \frac{2}{3V_{qg}}(\sigma_{\rm c} - P_{\rm in} - P_{\rm loss}) \tag{7}$$

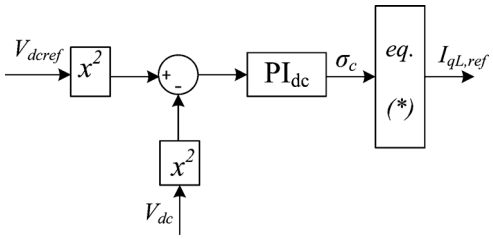

Fig. 4. Block diagram of the DC-link voltage controller.

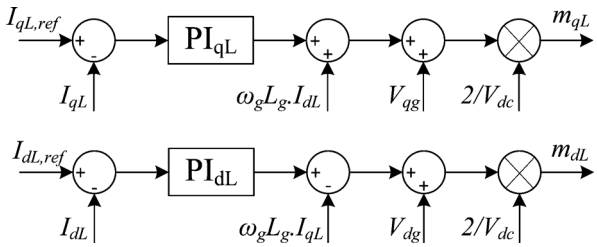

Fig. 5. Block diagram of the grid-side converter control loops.

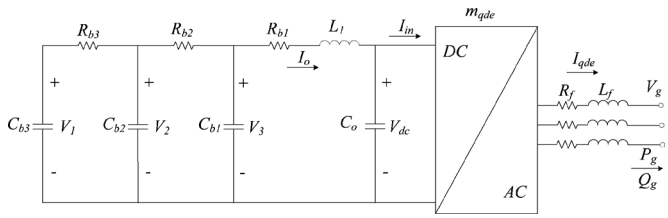

Fig. 6. Schematic diagram of an ECS unit.

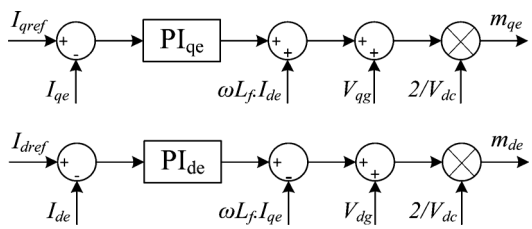

Fig. 7. Current control loops of the ECS.

b) Modeling of ECS Unit: Fig. 6 shows the schematic diagram of an ECS unit [20]. The control objectives for this unit are to regulate the output active and reactive powers of the unit through controlling the q- and d-axis components of the ECS output current (I_{qe} and I_{de}) according to (8) (current control loops are shown in Fig. 7):

$$\begin{cases} P_{\rm ref} = \dfrac{3}{2}|V_g|I_{q,\rm ref} \\ Q_{\rm ref} = -\dfrac{3}{2}|V_g|I_{d,\rm ref}. \end{cases} \tag{8}$$

The dynamic and algebraic equations of ECS unit derived from Fig. 6 are presented in Appendix C.

III. Calculating State-Space Matrices

Next step is to form the state-space equations of each component. For each synchronous generator, 7 dynamic state variables are added to the system. Also, four algebraic variables ($|V_i|, \theta_i$, I_{dmi} and I_{qmi}) are associated with the generator at Bus i. For a load at Bus i only two algebraic variables are added to the system ($|V_i|, \theta_i$).

Each PI-controller ($\mathrm{PI}(s) = k_p + k_i/s$) adds one dynamic state variable to the original state space equations. So, considering (1)–(6) and Figs. 1–3, there are a total of 12 dynamic state variables associated with each wind unit.[1] The state-space equations associated with PI-controllers are given in Appendix A.

In addition, each PI-controller adds one algebraic variable to the system. All the algebraic equations associated with wind unit are given in Appendix B.

Considering (36)–(42) (of Appendix C) and Fig. 7, each ECS unit has 11 state variables and three algebraic variables:

$$x_e = [\,V_1 \quad V_2 \quad V_3 \quad I_o \quad V_{\rm dc} \quad I_{qe} \quad I_{de} \quad x_P \quad x_Q \quad x_{qe} \quad x_{de}\,]^T$$
$$y_e = [\,I_{\rm in} \quad m_{qe} \quad m_{de}\,]^T.$$

Load switching disturbance is studied in this paper. Thus the disturbance vector, d, is defined as follows where N is the number of buses and N_w is the number of wind units:

$$d = [\,P_1 \quad \cdots \quad P_N \quad Q_1 \quad \cdots \quad Q_N\,].$$

Now that all state-space equations are formed, for studying the small signal analysis, they should be linearized around the steady-state point. After linearizing the combined Differential Algebraic Equations (DAE) related to the overall system we obtain the following:

$$\begin{bmatrix} \dot{x} \\ 0 \end{bmatrix} = \begin{bmatrix} A & B \\ D & E \end{bmatrix} \begin{bmatrix} x \\ y \end{bmatrix} + \begin{bmatrix} F \\ G \end{bmatrix} d \tag{9}$$

where x is the dynamic state vector and y is the algebraic variables vector. The matrices A, B, D, E, F, and G can be easily formed using the linearized equations. More details about linearizing the equations and forming the state-state matrix are presented in [17].

To solve this set of equations, they should be rewritten as standard state-space from which is obtained by eliminating y from equation below obtained from (9):

$$0 = Dx + Ey + Gd. \tag{10}$$

From (10) we obtain y as follows:

$$y = -E^{-1}(Dx + Gd). \tag{11}$$

After plugging (11) into (9), the following state-space equation is obtained:

$$\dot{x} = A_s x + B_s d \tag{12}$$

where

$$A_s = A - B(E^{-1}D) \tag{13}$$
$$B_s = F - B(E^{-1}G). \tag{14}$$

IV. Small Signal Analysis of Wind and ECS Units

For studying the effects of wind and ECS units on the small signal characteristics of overall power system we consider a wind unit together with an ECS unit connected to an infinite

[1] $x_w = [\omega_r \;\; I_{qs} \;\; I_{\rm ds} \;\; V_{\rm dc} \;\; I_{qL} \;\; I_{dL} \;\; x_\omega \;\; x_{qs} \;\; x_{\rm ds} \;\; x_{\rm dc} \;\; x_{qL} \;\; x_{dL}]^T$

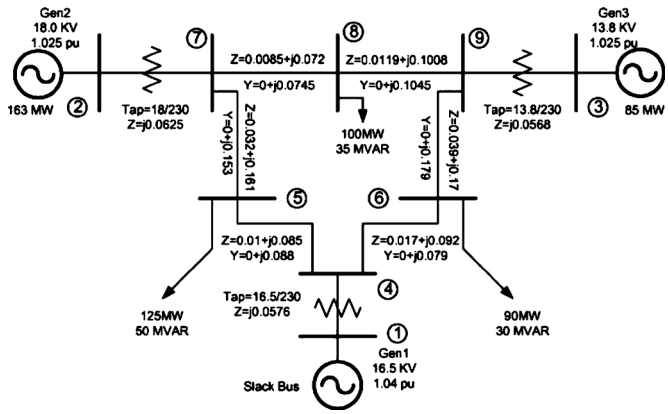

Fig. 8. Single line diagram of WSCC 9-bus system.

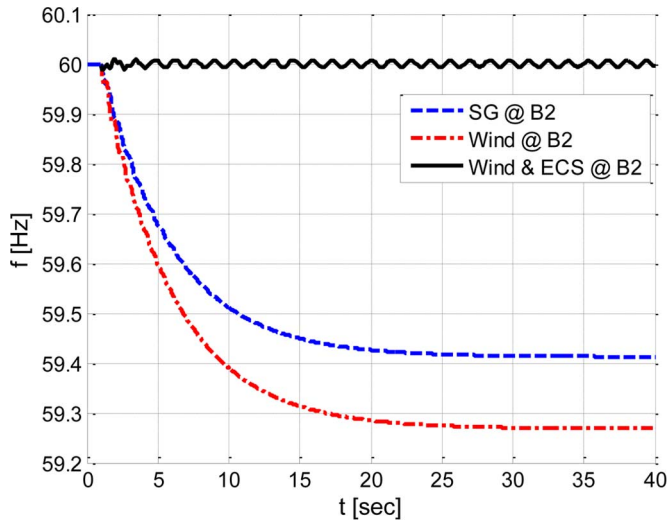

Fig. 9. Comparing the frequency of synchronous generator at Bus 1 to the load change.

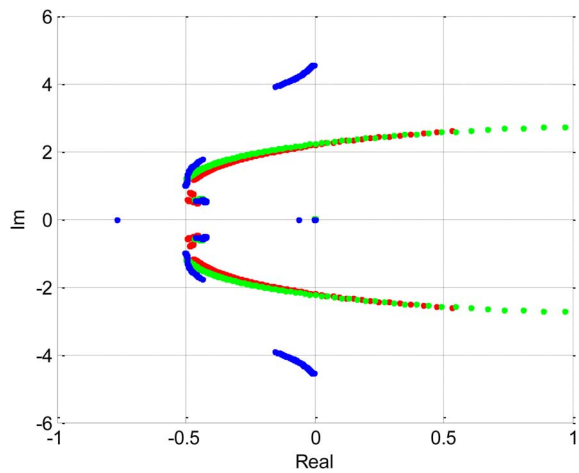

Fig. 10. Trajectory of EVs for the three test systems: S1—red dots, S2—green dots, and S3—blue dots.

bus. Turbine and generator data along with controller parameters of this wind unit are given in Appendix D. The data related to EDLC along with its controller is given in Appendix E. After finding state-space matrices, eigenvalues (EVs) of the wind unit, participant variables (PVs) and their participation factors (PFs) can be calculated. A participant variable (PV) associated to an eigenvalue (mode) is one that is significantly affected by that eigenvalue. Participation Factors (PFs) are dimensionless measure of state variable participation. PF of a state variable with respect to an eigenvalue is between zero and one. It shows the degree of interaction between the variable and the eigenvalue; larger the PF means more interaction between the state variable and the eigenvalue [17]. The list of Eigenvalues of the wind and ECS units, the participant variables and their participation factors are given in Appendix F.

V. Case Study

For investigating the small signal behavior of a power system including wind and ECS units, Western System Coordinating Council (WSCC) is used. This system has three synchronous generators and nine buses as shown in Fig. 8. The three generators are located at Buses 1, 2, and 3.

Eigenvalues of three different test systems are compared: S1) the original WSCC system with three conventional synchronous generators, S2) synchronous generator at Bus 2 is replaced with a wind unit and S3) synchronous generator at Bus 2 is replaced with a combined wind and ECS units. List of dominant EVs, PVs, and their PFs for these three test systems are shown below.

It can be inferred from the these tables that while wind unit participates in only two out of nine dominant EVs, state variables associated with ECS unit participates in four out of twelve dominant EVs. Also, it can be seen that ECS directly controls two zero EVs.

Fig. 9 shows the frequency of synchronous generator at Bus 1 for the three test systems for a step change (increase) in load at Bus 5. Comparing the steady state values of the three systems it can be seen that the system with wind unit (test system 2) experiences more frequency reduction than the system with all conventional synchronous generator (test system 1). This is to be expected as wind units, unlike conventional synchronous generators, do not possess governor. The figure also shows that when the ECS unit is added (test system 3), the steady-state error is almost zero. This is due to the fact that the ECS unit acts as an extremely fast governor and supports the added load. It should be noted that the effectiveness of ECS is for a short period of time since ECS cannot support the added load for more than a few minutes. It is reasonable to assume that the governors of the remaining synchronous generators will compensate for the load change for long term.

Now, to study the participation of state variables associated with unstable modes of each test system, the load at Bus 5 and generation of all generators (including the wind generator) are increased until the system becomes unstable (the amount of the load added to Bus 5 is divided between all generators in proportion to their inertia). Table IV shows the unstable EVs for the three test system and Fig. 10 shows the trajectories of EVs for these systems when load at Bus 5 increases from 1.25 pu to 4.62 pu (369.5% load increase).

The following can be concluded form the table.

1) As load and generations are increased, unstable EV-pair appears in all three systems. However, loadability of the

TABLE I
EVs, PVs, AND PFs OF WSCC (S1)

Eigenvalue	PVs	PFs
0	$\delta_1, \omega_1, \delta_2, \omega_2$	1, 0.99, 0.26, 0.25
0	$\delta_1, \omega_1, \delta_2, \omega_2$	1, 0.99, 0.26, 0.25
-0.191 ± j8.368	$\delta_2, \omega_2, \delta_1, \omega_1,$	1, 1, 0.42, 0.42
-0.455 + j0.464	$E_{q3}, R_{f3}, E_{q2}, R_{f2}$	1, 0.82, 0.35, 0.28
-0.472 ± j0.708	$E_{q1}, R_{f1}, E_{q2}, R_{f2}$	1, 0.76, 0.75, 0.59
-0.473 ± j1.166	$E_{q1}, R_{f1}, E_{q2}, R_{f2}, E_{q3}$	1, 0.72, 0.75, 0.55, 0.39
-0.719 ± j12.749	$\delta_3, \omega_3, \delta_2, \omega_2$	1, 1, 0.22, 0.22

TABLE II
EVs, PVs, AND PFs OF S2

Eigenvalue	PVs	PFs
0	$x_{\omega 2}, \omega_1, \omega_3, V_{dc2}, \omega_{r2}$	1, 0.78, 0.70, 0.36, 0.24
-0.198	E_{q3}, δ_1	1, 1
-0.304	$\omega_1, \omega_3, \delta_1, \delta_3, E_{q1}$	1, 0.72, 0.51, 0.51, 0.27
-0.469 ± j0.798	E_{q3}, R_{f3}	1, 0.78
-0.540 ± j11.225	ω_3, δ_3	1, 1
-1.075	$x_{\omega 2}, x_{dc}$	1, 0.89
-1.527	$E_{q3}, R_{f3}, R_{f1}, V_{r1}, E_{fd1}, E_{q1}, E_{d3}$	1, 0.78, 0.78, 0.61, 0.55, 0.26, 0.23

TABLE III
EVs, PVs, AND PFs OF S3

Eigenvalue	PVs	PFs
0	V_{1e2}, V_{2e2}	1, 0.96
0	V_{2e2}, V_{1e2}	1, 0.96
-0.063	V_{1e2}, V_{2e2}	1, 0.96
-0.105 ± j4.537	ω_1, δ_1	1, 1
-0.464 ± j0.556	R_{f1}	1
-0.503 ± j0.988	E_{q1}, R_{f1}	1, 0.75
-0.735 ± j12.472	ω_3, δ_3	1, 1
-0.767	V_{3e2}, R_{f3}	1, 0.96

TABLE IV
LIST OF UNSTABLE EVs OF THE THREE TEST SYSTEMS

System	L.I	Unstable EV	PVs	PFs
S1	*3.53*	*0.149 ± j2.35*	$E_{q2}, E_{q1}, R_{f2}, R_{f1}, E_{d2}, E_{d3}$	1, 0.96, 0.51, 0.48, 0.48, 0.35
S2	*3.26*	*0.119 ± j2.33*	E_{d3}, R_{f1}, R_{f3}	1, 0.41, 0.36
S3	*3.70*	*762.4 ± j6761*	$I_{dL2}, I_{qe2}, I_{qL2},$	1, 0.70, 0.70

system decreases when a synchronous generator (SG) is replaced by a wind unit.

2) In the system with SGs and wind units (S2), EVs associated with SGs are causing the instability, while in the system with SGs, wind generation, and ECS unit (S3) unstable EVs are associated with ECS and wind units.
3) ECS unit can increase the loadability of the system. The loadability of a system with combined wind and ECS is even larger than a system without wind unit (it should be noted that in the case of a system with only synchronous generator and ECS unit, loadability is higher than S3 and L.I before instability is 3.84).

TABLE V
UNSTABLE EV FOR S3 AFTER LOAD INCREASE

Load Increase	Unstable EV	PVs	PFs
3.695	*762.4 ± j6761*	$I_{dL2}, I_{qe2}, I_{qL2},$	1, 0.70, 0.70
3.7	*3780.5*	$I_{qe2}, I_{qL2}, I_{dL2}$	1, 0.60, 0.56
3.8	*1298.4*	$I_{qe2}, x_{dL2}, I_{dL2}$	1, 0.58, 0.47
	0.261 ± j2.428	$E_{q1}, E_{d3}, \delta_1, \omega_1, E_{q3}, R_{f1}$	1, 0.68, 0.63, 0.62, 0.60, 0.47
3.9	*501.50*	$I_{qe2}, I_{de2}, I_{ds2}, x_{ds2}$	1, 0.85, 0.84, 0.38
	1.198 ± j2.304	$E_{q1}, \delta_1, \omega_1, E_{d3}, E_{q3}, R_{f1}$	1, 0.81, 0.78, 0.75, 0.58, 0.37
4.0	*153.43*	$I_{de2}, I_{qe2}, x_{de2}, x_{qe2}, I_{ds2}, x_{P2}$	1, 0.82, 0.61, 0.61, 0.59, 0.42
	4.323	$E_{q1}, \delta_1, E_{d3}, \omega_1, E_{q3}$	1, 0.92, 0.91, 0.46, 0.35
	2.255	ω_1, δ_1	1, 0.76
4.1	*0.745*	E_{q1}, E_{q3}, R_{f3}	1, 0.64, 0.38
4.2	*0.104*	R_{f1}	1
4.21	*System is stable*		
4.3	*Power flow does not converge*		

We now focus on test system three (S3) which includes conventional generators, wind generation system and energy storage unit. Two extensive studies are carried out for this system:

a) Hopf Bifurcation: For S3 the load at Bus 5 is increased until the power flow diverges. Table V shows the unstable EVs for various loads and the associated participant variables and participation factors. It shows that the first unstable EV is controlled by wind and ECS units at Bus 2. For a load increase of 3.8, another unstable EV is appeared which is controlled solely by the synchronous generators.

b) Hopf Bifurcation and Trajectory of Unstable EVs: Fig. 11 shows the trajectory of EVs near the origin for load changes from 1 pu to 4.2 pu. Hopf bifurcation (HB) points are shown in this figure.

Fig. 12 shows the P-V curve for Bus 5. Hopf bifurcation point and singularity-induced bifurcation point are shown in this graph.

VI. CONCLUSION

In this paper, small signal stability of a power system including wind and ECS units was studied and compared with two other systems: a system with only conventional sources and a system with wind generation but without any ECS unit. Also, effect of loading on unstable modes of this system was investigated.

The results show that while replacing a synchronous machine with a wind unit has negative effect on loadability of the system,

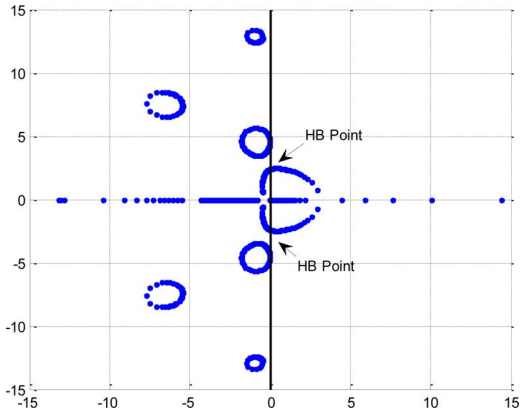

Fig. 11. Trajectory of EVs near the origin.

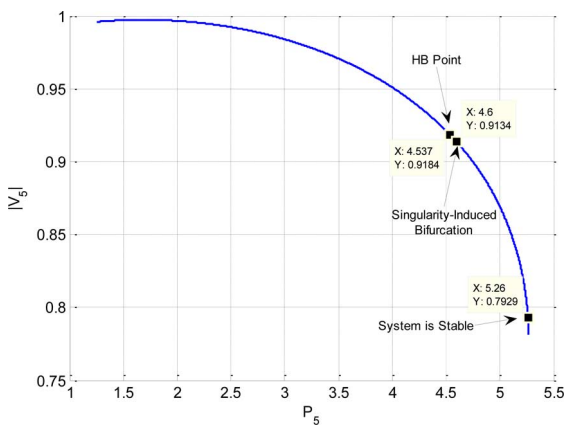

Fig. 12. PV curve for Bus 5.

addition of ECS unit can increase the loadability (or transmission capacity). The increased loadability is even more than the original system having synchronous generators only. In addition, from the simulation results it was found that wind units (in a system without ECS) do not participate at unstable modes (or eigenvalue) of the system, but after adding ECS unit to the system both ECS and wind units cause unstable eigenvalues.

In common practice (as reported in literature), the main purpose of using ECS unit is to smooth the output power of wind units. Based on the results of this research, it can be concluded that adding ECS can also enhance the stability and/or loadability of the overall system. This is an additional benefit of using ECS together with wind generation.

APPENDIX

A. Appendix A—Dynamic Equations of PI-Controllers Associated With Wind Unit

$$sx_{\omega} = k_{i\omega}(\omega_{r,\mathrm{ref}} - \omega_r) \tag{15}$$
$$sx_{\mathrm{ds}} = k_{i\mathrm{ds}}(I_{\mathrm{ds,ref}} - I_{\mathrm{ds}}) \tag{16}$$
$$sx_{qs} = k_{iqs}(I_{qs,\mathrm{ref}} - I_{qs}) \tag{17}$$
$$sx_{\mathrm{dc}} = k_{i\mathrm{dc}}(V^2_{\mathrm{dc,ref}} - V^2_{\mathrm{dc}}) \tag{18}$$
$$sx_{qL} = k_{iqL}(I_{qL,\mathrm{ref}} - I_{qL}) \tag{19}$$
$$sx_{dL} = k_{idL}(I_{dL,\mathrm{ref}} - I_{dL}). \tag{20}$$

B. Appendix B—Algebraic Equations of Wind Unit

The following are the algebraic equations associated with each wind unit. In total there are 15 algebraic variables[2]

$$0 = k_{p\omega}(\omega_{r,\mathrm{ref}} - \omega_r) + x_{\omega} - T_m - T_e - \frac{2J}{P} I_{qs,\mathrm{ref}} \tag{21}$$
$$0 = k_{pqs}(I_{qs,\mathrm{ref}} - I_{qs}) + x_{qs} + \omega_e L I_{\mathrm{ds}} + \frac{\omega_r L_m}{L_r}\lambda_r - \frac{1}{2} m_{qs} V_{\mathrm{dc}} \tag{22}$$
$$0 = k_{pds}(I_{\mathrm{ds,ref}} - I_{\mathrm{ds}}) + x_{\mathrm{ds}} - \omega_e L I_{qs} - \frac{R_r L_m}{L_r^2}\lambda_r - \frac{1}{2} m_{\mathrm{ds}} V_{\mathrm{dc}} \tag{23}$$
$$0 = k_{pdc}(V^2_{dcref} - V^2_{\mathrm{dc}}) + x_{\mathrm{dc}} - P_{\mathrm{in}} - P_{\mathrm{loss}} - \frac{3}{2}|V_g| I_{qL,\mathrm{ref}} \tag{24}$$
$$0 = Q_{\mathrm{ref}} + \frac{3}{2}|V_g| I_{dL,\mathrm{ref}} \tag{25}$$
$$0 = k_{pqL}(I_{qLr,\mathrm{ref}} - I_{qL}) + x_{qL} + \omega_g L_f I_{dL} + |V_g| - \frac{1}{2} m_{qL} V_{\mathrm{dc}} \tag{26}$$
$$0 = k_{pdL}(I_{dLr,\mathrm{ref}} - I_{dL}) + x_{dL} - \omega_g L_f I_{qL} - \frac{1}{2} m_{dL} V_{\mathrm{dc}} \tag{27}$$
$$0 = \frac{2}{P} T_m \omega_r - \frac{1}{2}\rho A C_p V_w^3 \tag{28}$$
$$0 = T_e - \frac{3P}{4}\frac{L_m}{L_r}\lambda_r I_{qs} \tag{29}$$
$$0 = L_r \lambda_r \omega_e - L_r \lambda_r \omega_r - R_r L_m I_{qs} \tag{30}$$
$$0 = \omega_{r,\mathrm{ref}} - \frac{P}{2}\frac{N_g \lambda_{\mathrm{opt}}}{R_t} V_w \tag{31}$$
$$0 = P_{\mathrm{in}} + \frac{3}{4} V_{\mathrm{dc}}(m_{qs} I_{qs} + m_{\mathrm{ds}} I_{\mathrm{ds}}) \tag{32}$$
$$0 = P_{\mathrm{loss}} - \frac{3}{2} R_g (I_{qL}^2 + I_{dL}^2) \tag{33}$$
$$0 = \omega_r - \frac{P}{2}\frac{N_g}{R_t}\lambda V_w \tag{34}$$
$$0 = C_p - 0.5(\lambda - 0.022\beta^2 - 5.6)e^{-0.17\lambda}. \tag{35}$$

C. Appendix C—Dynamic and Algebraic Equations of ECS

$$sV_1 = -\frac{1}{C_{b3}}\frac{V_1 - V_2}{R_{b3}} \tag{36}$$
$$sV_2 = \frac{1}{C_{b2}}\left(\frac{V_1 - V_2}{R_{b3}} - \frac{V_2 - V_3}{R_{b2}}\right) \tag{37}$$
$$sV_3 = \frac{1}{C_{b1}}\left(\frac{V_2 - V_3}{R_{b2}} - I_o\right) \tag{38}$$
$$sI_o = \frac{1}{L_1}(V_3 - R_{b1} I_o - V_{\mathrm{dc}}) \tag{39}$$
$$sV_{\mathrm{dc}} = \frac{1}{C_o}(I_o - I_{\mathrm{in}}) \tag{40}$$
$$sI_{qL} = \frac{1}{L_f}\left(\frac{m_{qe}}{2} V_{\mathrm{dc}} - R_f I_{qe} - \omega_g L_f I_{de} - |V_g|\right) \tag{41}$$
$$sI_{dL} = \frac{1}{L_f}\left(\frac{m_{de}}{2} V_{\mathrm{dc}} - R_f I_{de} + \omega_g L_f I_{qe}\right). \tag{42}$$

[2] $y_w = [\omega_{r,\mathrm{ref}} \;\; I_{qs,\mathrm{ref}} \;\; I_{\mathrm{ds,ref}} \;\; T_m \;\; T_e \;\; m_{qs} \;\; m_{\mathrm{ds}} \;\; \omega_e \;\; \cdots \;\; m_{qL} \;\; m_{dL} \;\; V_g \;\; V_{dcref} \;\; P_{\mathrm{in}} \;\; P_{\mathrm{loss}} \;\; I_{qL.ref} \;\; I_{dL,\mathrm{ref}}]^T$.

TABLE VI
WIND TURBINE DATA AND GENERATOR DATA

$R_t = 54\ m$	$\rho = 1.225\ kg/m^3$	$N_g = 37$
$J = 2\ kg.m^2$	$R_s = 1.102\ m\Omega$	$R_r = 1.497\ m\Omega$
$L_{ls} = 0.06492\ mH$	$L_{lr} = 0.06492\ mH$	$L_m = 2.13461\ mH$
$\lambda_r = 1.74\ Wb$	$R_g = 0.002\ \Omega$	$L_g = 0.15\ mH$

TABLE VII
CONTROLLER DATA FOR ALL CONTROLLER LOOPS USED FOR MODELING THE WIND UNIT

$K_{p\omega} = 0.3889$	$K_{i\omega} = 0.075626$	$K_{pP} = 15.556$
$K_{iP} = 121$	$T = 0.2$	$K_{pr} = 194.45$
$K_{ir} = 18900$	$K_{pqs} = 0.0852$	$K_{iqs} = 30.09$
$K_{pds} = 0.0852$	$K_{ids} = 30.09$	$K_{pdc} = 1.4849$
$K_{idc} = 16.75$	$K_{pqL} = 0.2025$	$K_{iqL} = 304.5925$
$K_{pdL} = 0.2025$	$K_{idL} = 304.5925$	

TABLE VIII
ECS PARAMETERS USED IN ALL THE SIMULATIONS

$R_{b1} = 0.03125\ \Omega$	$R_{b2} = 0.78125\ \Omega$	$R_{b3} = 0.75\ \Omega$	$L_1 = 0.001\ H$
$C_{b1} = 1.68\ F$	$C_{b2} = 42\ F$	$C_{b3} = 40.32\ F$	$C_o = 60\ mF$

TABLE IX
EVS, PVS, AND PFS OF THE WIND UNIT

Eigenvalue	PVs	PFs
-7.13	I_{ds}, V_{dc}, x_{ds}	1, 0.84, 0.31
-7.34 ± j11.18	ω_r, x_ω	1, 1
14.17	I_{ds}, V_{dc}, x_{ds}	1, 0.83, 0.30
-342.83 ± j343.05	$x_{dL}, x_{ds}, I_{ds}, I_{dL}$	1, 0.83, 0.48, 0.48
-351.70	ω_r, x_{qs}	1, 0.3
-656.69 ± j1257.67	$I_{qL}, x_{qs}, x_{qL}, I_{qs}$	1, 1, 0.98, 0.29
-681.67 ± j 1251.4	x_{dc}	1
-5063.0	I_{qs}	1

TABLE X
EVS, PVS, AND PFS OF ECS UNIT

Eigenvalue	PVs	PFs
0.0000	x_Q	1
0.0000	x_{de}	1
0.0000	x_Q	1
-0.0634	V_1, V_2	1, 0.96
-0.767	x_{qe}, V_3, V_{dc}	1, 0.94, 0.55
-15.64 ± j130.45	V_3, V_{dc}	1, 1
-77.78 ± j77.78	V_{dc}, V_3	1,0.89
-77.78 ± j77.78	I_o, V_{dc}	1, 0.67

For PI_{qe} and PI_{de} the following dynamic equations are added to the system:

$$sx_{qe} = k_{iqe}(I_{qe,\mathrm{ref}} - I_{qe}) \tag{43}$$

$$sx_{de} = k_{de}(I_{de,\mathrm{ref}} - I_{de}). \tag{44}$$

Three algebraic equations are associated with the ECS unit. These equations are

$$0 = I_{\mathrm{in}} - \frac{3}{4}(m_{qe}I_{qe} + m_{de}I_{de}) \tag{45}$$

$$0 = x_{qe} + k_{pqe}(I_{qe,\mathrm{ref}} - I_{qe}) + \omega_g L_f I_{de} + |V_g| - \frac{m_{qe}}{2}V_{\mathrm{dc}} \tag{46}$$

$$0 = x_{de} + k_{pde}(I_{de,\mathrm{ref}} - I_{de}) - \omega_g L_f I_{qe} - \frac{m_{de}}{2}V_{\mathrm{dc}}. \tag{47}$$

D. Appendix D—Wind Unit Data

Table VI is wind turbine data and generator data.

Also, Table VII lists controller data for all controller loops used for modeling the wind unit.

E. Appendix E—ECS Unit Data

Table VIII lists ECS parameters used in all the simulations.

F. Appendix F—EVs, PVs, and PFs of Wind and ECS Unit

Table IX lists the EVs, PVs, and PFs of the wind unit, and Table X lists the EVs, PVs, and PFs of ECS unit.

REFERENCES

[1] International Energy Statistics EIA's Portal for Detailed Country and Regional Energy Data [Online]. Available: http://tonto.eia.doe.gov/cfapps/ipdbproject/IEDIndex3.cfm

[2] C. Abbey and G. Joos, "Supercapacitor energy storage for wind energy applications," *IEEE Trans. Ind. Applicat.*, vol. 43, pp. 769–776, 2007.

[3] T. K. A. Brekken, A. Yokochi, A. von Jouanne, Z. Z. Yen, H. M. Hapke, and D. A. Halamay, "Optimal energy storage sizing and control for wind power applications," *IEEE Trans. Sustain. Energy*, vol. 2, pp. 69–77, 2011.

[4] G. O. Cimuca, C. Saudemont, B. Robyns, and M. M. Radulescu, "Control and performance evaluation of a flywheel energy-storage system associated to a variable-speed wind generator," *IEEE Trans. Ind. Electron.*, vol. 53, pp. 1074–1085, 2006.

[5] J. S. Derk, "Compressed air energy storage in an electricity system with significant wind power generation," *IEEE Trans. Energy Convers.*, vol. 22, pp. 95–102, 2007.

[6] B. Hartmann and A. Dan, "Cooperation of a grid-connected wind farm and an energy storage unit—Demonstration of a simulation tool," *IEEE Trans. Sustain. Energy*, vol. 3, pp. 49–56, 2012.

[7] L. Ming-Shun, C. Chung-Liang, L. Wei-Jen, and W. Li, "Combining the wind power generation system with energy storage equipment," *IEEE Trans. Ind. Applicat.*, vol. 45, pp. 2109–2115, 2009.

[8] M. G. Molina and P. E. Mercado, "Power flow stabilization and control of microgrid with wind generation by superconducting magnetic energy storage," *IEEE Trans. Power Electron.*, vol. 26, pp. 910–922, 2011.

[9] S. Teleke, M. E. Baran, S. Bhattacharya, and A. Q. Huang, "Optimal control of battery energy storage for wind farm dispatching," *IEEE Trans. Energy Convers.*, vol. 25, pp. 787–794, 2010.

[10] S. Teleke, M. E. Baran, A. Q. Huang, S. Bhattacharya, and L. Anderson, "Control strategies for battery energy storage for wind farm dispatching," *IEEE Trans. Energy Convers.*, vol. 24, pp. 725–732, 2009.

[11] J. Kumagai, "A battery as big as the grid," *IEEE Spectrum*, vol. 49, pp. 45–46, 2012.

[12] R. Cardenas, R. Pena, G. Asher, and J. Clare, "Power smoothing in wind generation systems using a sensorless vector controlled induction machine driving a flywheel," *IEEE Trans. Energy Convers.*, vol. 19, pp. 206–216, 2004.

[13] G. O. Suvire and P. E. Mercado, "Active power control of a flywheel energy storage system for wind energy applications," *IET Renew. Power Gener.*, vol. 6, pp. 9–16, 2012.

[14] A. Uehara *et al.*, "A coordinated control method to smooth wind power fluctuations of a PMSG-based WECS," *IEEE Trans. Energy Convers.*, vol. 26, pp. 550–558, 2011.

[15] T. C. Yang, "Initial study of using rechargeable batteries in wind power generation with variable speed induction generators," *IET Renew. Power Gener.*, vol. 2, pp. 89–101, 2008.

[16] S. M. Muyeen, T. Murata, and J. Tamura, *Stability Augmentation of a Grid-Connected Wind Farm*. London, U.K.: Springer-Verlag, 2008.

[17] P. W. Sauer and M. A. Pai, *Power System Dynamics and Stability*. Englewood Cliffs, NJ, USA: Prentice Hall, 1998.

[18] *IEEE Recommended Practice for Excitation System Models for Power System Stability Studies*, IEEE Std. 421.5-1992, 1992.

[19] P. M. Anderson and A. Bose, "Stability simulation of wind turbine systems," *IEEE Trans. Power App. Syst.*, vol. PAS-102, pp. 3791–3795, 1983.

[20] A. Jamehbozorg and G. Radman, "Enhancement of micro-grid dynamics in presence of wind units using energy capacitor systems," in *Proc. North American Power Symp. (NAPS), 2012*, 2012, pp. 1–6.

[21] W. Bin, L. Yongqiang, and K. Samir, *Power Conversion and Control of Wind Energy Systems*. New York, NY, USA: Wiley, 2011.

Arash Jamehbozorg received the B.S. and M.S. degrees in electrical engineering from Iran University of Science and Technology (IUST), Iran, in 2005 and 2008, respectively, and the Ph.D. degree from Tennessee Technological University, Cookeville, TN, USA, in 2013.

Currently, he is an Assistant Professor of electrical engineering at California State University, Los Angeles, CA, USA. His research interests include renewable energy sources, storage units, dynamics of power systems, and mathematical modeling of power systems.

Ghadir Radman received the Ph.D. degree in electrical engineering from Tennessee Technological University, Cookeville, TN, USA.

He is currently a Professor of electrical engineering at Tennessee Technological University. His research interests include power system dynamics, power flow control, FACTS, distributed generations, smart grid, and large-scale systems.

Prof. Radman is a senior member of the IEEE Power & Energy Society.